2698–2709 *Nucleic Acids Research, 2006, Vol. 34, No. 9*
doi:10.1093/nar/gkl318

Affinity of molecular interactions in the bacteriophage ϕ29 DNA packaging motor

Mark A. Robinson[1,3], Jonathan P.A. Wood[1,3], Stephanie A. Capaldi[1,3], Andrew J. Baron[1,3], Christopher Gell[2,3], D. Alastair Smith[2,3] and Nicola J. Stonehouse[1,3,*]

[1]Institute of Molecular and Cellular Biology, Faculty of Biological Sciences, [2]Institute of Molecular Biophysics and [3]Astbury Centre for Structural Molecular Biology, University of Leeds, Leeds, LS2 9JT, UK

Received March 16, 2006; Revised April 4, 2006; Accepted April 12, 2006

ABSTRACT

DNA packaging in the bacteriophage ϕ29 involves a molecular motor with protein and RNA components, including interactions between the viral connector protein and molecules of pRNA, both of which form multimeric complexes. Data are presented to demonstrate the higher order assembly of pRNA together with the affinity of pRNA:pRNA and pRNA:connector interactions, which are used to propose a model for motor function. In solution, pRNA can form dimeric and trimeric multimers in a magnesium-dependent manner, with dissociation constants for multimerization in the micromolar range. pRNA:connector binding is also facilitated by the presence of magnesium ions, with a nanomolar apparent dissociation constant for the interaction. From studies with a mutant pRNA, it appears that multimerization of pRNA is not essential for connector binding and it is likely that connector protein is involved in the stabilization of higher order RNA multimers. It is proposed that magnesium ions may promote conformational change that facilitate pRNA:connector interactions, essential for motor function.

INTRODUCTION

The bacteriophage ϕ29 of *Bacillus subtilis* packages its genomic dsDNA in an ATP-dependent fashion, with components of the virus forming a powerful molecular motor (Figure 1A) (1,2). The viral procapsid (prohead) is composed of the capsid proteins with an associated connector (portal). Packaging of the viral genomic dsDNA (covalently complexed with gp3) involves the presence of RNA molecules (pRNA) and hydrolysis of ATP by an associated ATPase (gp16) (3).

DNA packaging as a result of symmetry-mismatch between viral components was first proposed in the 1970s (4) and the model relies on those components having mismatched symmetries in order to reduce the energy barrier to rotation. Although it is also possible that packaging occurs without rotation of subunits of the motor, for example by employing a ratchet-based mechanism (5), many studies aiming to elucidate motor function have focused on attempting to ascertain the stoichiometry of ϕ29 components. It is now clear that the connector exists as a dodecamer of gp10 molecules (6–9), therefore these studies have concentrated on the stochiometry of pRNA. It has been previously reported that the termini of full-length 174 nt pRNA can be shortened to yield 120 nt pRNA (Figure 1B) and that both forms are competent in viral assembly *in vitro* (10). The predicted secondary structure of pRNA incorporates four bases in the CE loop (45-AACC-48) that are complementary to four bases in the D loop (82-GGUU-85). The possibility that base pairing between adjacent pRNA molecules is involved in the tertiary structure of pRNA has been investigated through the mutation of these loop sequences (11) and as a consequence, there have been many reports on the multimeric nature of pRNA in DNA packaging. Experiments from both the Anderson and Guo laboratories demonstrated that mutant pRNAs could be designed to form closed hexameric rings as complementary monomers, dimers or trimers (12,13). Open hexamers were shown to be inactive in *in vitro* packaging assays (13). This is compelling evidence for the involvement of closed hexamers, yet it does not exclude the possibility that

*To whom correspondence should be addressed. Tel: + 44 113 343 3102; Fax: + 44 113 343 2835; Email: n.j.stonehouse@leeds.ac.uk
Present addresses:
Jonathan P.A. Wood, Materials Today, Elsevier, The Boulevard, Langford Lane, Kidlington, OX5 1GB, UK
Stephanie A. Capaldi, Massachusetts Institute of Technology, Department of Biology, 31 Ames Street, 68-132 Cambridge MA 02139, USA

The authors wish it to be known that, in their opinion, the first two authors should be regarded as joint First Authors

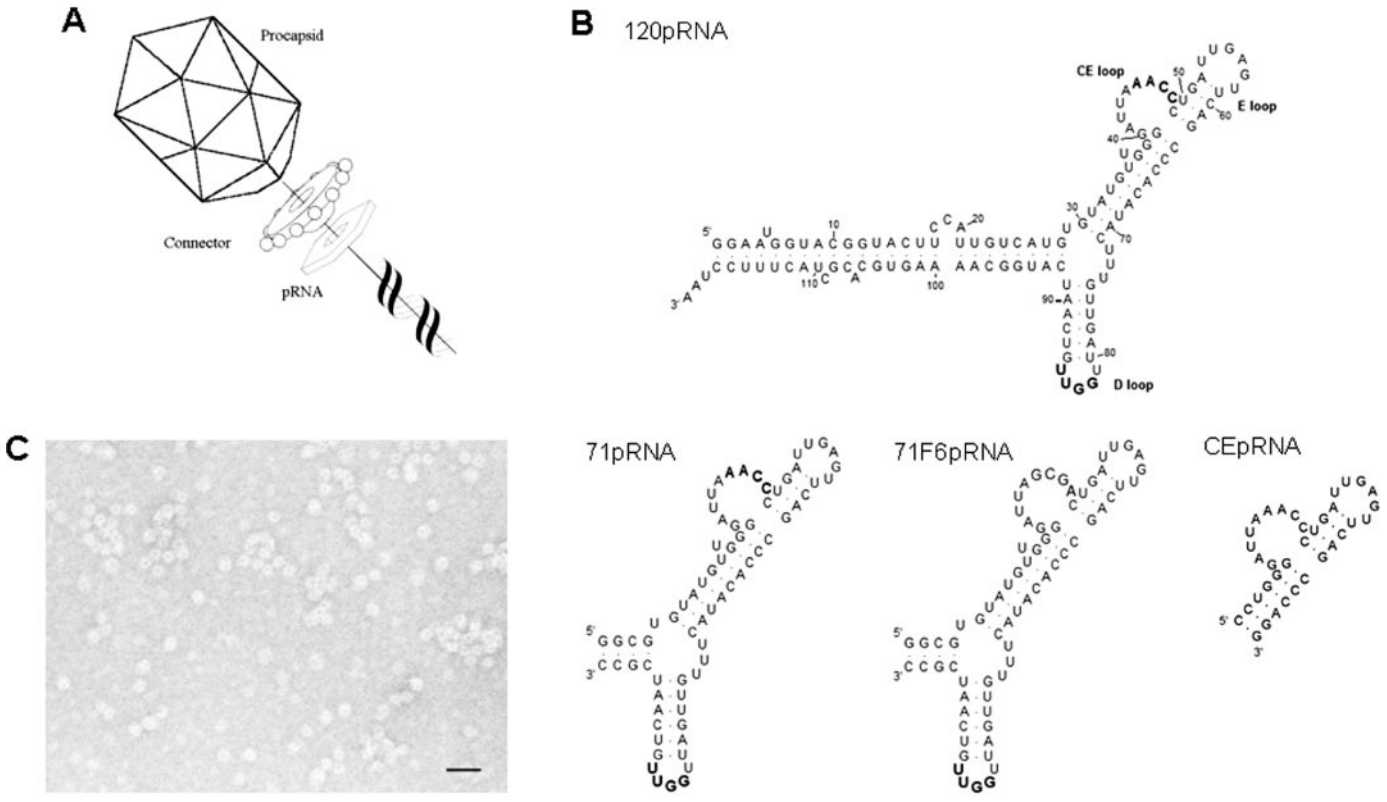

Figure 1. Schematic representation of the components of bacteriophage ϕ29 during packaging of genomic dsDNA (**A**). The predicted secondary structure of ϕ29 pRNA sequences used in this study (**B**), as calculated by MFold (38,39). 120pRNA is a 120mer that retains full ϕ29 genomic dsDNA packaging activity, but is shorter than the wild-type ϕ29 174mer pRNA. Complementary bases in the CE and D loops implicated in pRNA multimerization are in bold. 71pRNA is a shortened version of 120pRNA, with identical loop structure, whilst 71F6pRNA is modified to remove base pairing between CE and D loops. Neither 71pRNA nor 71F6pRNA are competent to package ϕ29 genomic dsDNA. The CEpRNA region, used in the SMPB experiments in this study, is a truncated non-multimerizing variant. TEM analysis of C-His gp10 (**C**) indicates assembly into structures with dimensions and appearance similar to previously published data for the wild-type protein. Size bar = 40 nm.

other 'closed' multimers could have a role in the packaging event. Cryo-electron microscopy (cryo-EM) investigations of prohead structure before and after RNase treatment (8,14) have indicated the presence of density for RNA protruding from the funnel-shaped connector. Reconstruction of 3D structures from 2D projections allowed analysis of 5-fold and 6-fold symmetries along the longitudinal axis of the connector. In one study, superimposition of a 6-fold symmetry resulted in the retention of gp10 connector and pRNA features (14). This is in contrast to the work of Simpson *et al*. (8) where pRNA density was consistent with imposed 5-fold symmetry. The issue of pRNA stoichiometry therefore appears to be unresolved, and it has been postulated that both pRNA hexamers and pentamers could play a role in DNA packaging, with the former involved in initial binding, followed by the loss of one molecule resulting in a functional pentamer (8).

We have taken a different approach in order to provide information essential for the rational elucidation of the mechanism of DNA packaging, based on determination of the affinity between components. The presence of solution state multimers of pRNA, formed by multimerization in the absence of other ϕ29 components, has been analysed by light scattering experiments. Further analysis of pRNA multimerization has been achieved using analytical ultracentrifugation (AUC), leading to data for the affinity of the solution state pRNA:pRNA interaction under a range of magnesium ion concentrations. Single molecule photobleaching (SMPB) experiments, in which the photobleaching of individual fluorophore-labelled pRNA molecules is monitored, have been used to further confirm the ability of pRNA to form higher order assemblies and also probe the effect of the presence of connector on pRNA multimerization. Further analysis of the components of the packaging system has been achieved by an investigation of the affinity of pRNA for connector gp10 using bead-based binding affinity assays. The role of intermolecular base pairing of pRNA in the formation of higher order multimeric forms has been probed in all experiments by the comparison of wild-type and multimerization-incompetent mutant pRNAs.

MATERIALS AND METHODS

General

Chemicals and reagents were from BDH Merck Ltd, Dharmacon Inc., Fisher Chemicals, ICN, Oxoid, Promega

Corporation, Severn Biotech Ltd, or Sigma. Enzymes were from Promega Corporation.

Preparation of RNA

Four RNA species (Figure 1B) were used in this study. 120pRNA is a shortened wild-type sequence that maintains a DNA packaging activity equivalent to that of the wild-type 174mer pRNA (10,15). 71pRNA represents bases 25–95 of 120pRNA, resulting in a shortened A helix, whilst maintaining its potential to form intermolecular base pairs and bind to the viral prohead (11). 71F6pRNA is a derivative of 71pRNA with mutations in bases 45–48 of the CE loop. This is predicted to result in the loss of ability to intermolecularly base pair with the D loop, based on the behaviour of the previously published F6 variant of 120pRNA (11). CEpRNA is a small RNA fragment based on pRNA but with the D loop removed entirely, preventing formation of intermolecular interactions.

DNA templates for the *in vitro* transcription of 71pRNA and 120pRNA (pGEM-T Easy 71pRNA and pGEM-T Easy 120pRNA) were prepared by the ligation of a PCR-produced template into pGEM-T Easy (Promega Corporation). A DNA template for the *in vitro* transcription of 71F6pRNA (pGEM-T Easy 71F6) was prepared by the site-specific PCR mutation of plasmid pGEM-T Easy 71pRNA; the 4 bp coding AACC in the CE loop of 71pRNA in pGEM-T Easy 71pRNA were mutated to GCGA. The identity of all clones was confirmed by the DNA sequencing facility at the University of Durham, UK. The RNAs were produced by T7 *in vitro* transcription and purified by denaturing PAGE. The molecular weight (MW) of RNA species was confirmed using electrospray ionisation mass spectrometry (ESI-MS) following concentration and desalting (16): 71pRNA observed MW 22 966 Da, expected MW 22 967 Da; 71F6pRNA observed MW 23 024 Da, expected MW 23 023 Da; 120pRNA observed MW 38 685 Da, expected MW 38 639 Da, consistent with M + $2Na^+$ (38 685 Da). ^{32}P-labelled RNA was prepared by the addition of uridine 5′-[α-^{32}P]triphosphate (Amersham Biosciences) to *in vitro* transcription reactions.

N-71pRNA and N-CEpRNA were synthesized using solid-phase 2′-ACE phosphoramidite chemistry (Dharmacon Inc.) (17). Purification was achieved by high pressure liquid chromatography (HPLC) on a DNAPac PA100 column (Dionex) eluting with a 0 → 1 M NaCl gradient at 65°C. Samples were desalted using a HiPrep 26/10 Desalting Column (Amersham Biosciences), eluting with H_2O. Alexa Fluor 488 was conjugated to amine-modified RNA using the 2,3,5,6-tetrafluoro-phenyl ester strategy according to the manufacturers' instructions (Molecular Probes). Purification was achieved by HPLC as described above, allowing separation of the AlexaFluor 488 labelled RNA from unlabelled RNA, resulting in AF-N-71pRNA and AF-N-CEpRNA.

Preparation of C-His gp10

In previous cryo-EM reconstruction studies of assembling phage particles, putative pRNA density was located at the narrow end of the connector (8,14). Although missing from both crystal structures (8,9), it appears that the C-termini of gp10 connectors are likely to be located in the wide region of the structure, remote from the pRNA binding region. In order to ensure that connectors with the pRNA binding site exposed could be readily prepared at high purity for use in our experiments, a construct was designed to express gp10 with a C-terminal hexa-histidine tag (C-His gp10). Samples of this protein were investigated by transmission electron microscopy (TEM) (Figure 1C) and shown to assemble into structures with dimensions and appearance equivalent to previously published data for the wild-type protein (18).

PCR was used to replicate the gp10 gene from plasmid pAR7-8-8.5-10 (19) and incorporate a C-terminal hexa-histidine tag to form plasmid pET-21a (+) C-gp10. Over-expression in BL21 (DE3) cells (Novagen) resulted in a cell pellet that was resuspended in 50 mM NaH_2PO_4, 300 mM NaCl, 10 mM imidazole (pH 7.0). Lysozyme (1 mg ml^{-1}), DNase I (10 μg ml^{-1}), RNase A (5 μg ml^{-1}), $MgCl_2$ (6 mM) and a Complete™ EDTA free Protease Inhibitor Cocktail tablet were added before sonication. C-His gp10 was purified from the supernatant by Nickel-affinity chromatography. The MW of C-His gp10 was accurately determined to within 0.01% of the calculated MW using ESI-MS (observed MW 36 815 Da, expected MW 36 812 Da). Samples were visualized by TEM by immobilization onto formvar/carbon-coated copper grids, staining with 4% uranyl acetate and imaged at 50 000× magnification at 80 kV (20).

DLS

Dynamic light scattering (DLS) measurements were performed using a PDDLS/Batch light scattering platform and a PD2000DLS detector (Precision Detectors) in a temperature controlled Friocell unit (Camlab). A 200 μl sample of RNA (0.02 μm filtered, final concentration 0.75–1 mg ml^{-1}) was placed in a microcuvette (Polymer Labs) and equilibrated at 14°C before use. $MgCl_2$ (10 mM) was added and measurements taken after 3 and 16 h. Filtered EDTA (10 mM) was added and incubated for 2–3 h and DLS data recorded. At each point in the experiment, ten separate measurements of the intensity correlation function were made. Each measurement used a sample time of 4–5 μs, a run time of 1 s, and the accumulation of 100 runs. The average photon count rate was between 4×10^5 and 8×10^5 counts s^{-1}, ensuring that multiple scattering was not a significant factor. A threshold filter was employed to eliminate individual runs from the accumulation where the count rate was vastly increased, as this was assumed to be due to the temporary presence of large dust particles in the laser beam. Data analysis revealed baseline fluctuations to be small and the average deviation in the size distribution fit to the correlation function to be 1–3%. Size distributions from individual measurements were averaged. Data were analysed using Precision Deconvolve software (Precision Detectors).

SEC-LS

The size exclusion chromatography with online light scattering and ultraviolet (UV) absorbance detection (SEC-LS) system comprised a LC1120 HPLC pump (Polymer Labs), a 30 × 8 mm Diol size exclusion column with 200 Å pore size (YMC) in a controlled temperature Friocell unit (Camlab) and PD2010 in-line 90° light scattering (Precision Detectors) and LC1200 UV-visible (Polymer Laboratories)

detectors. 71F6pRNA was used to calibrate the inter-detector volume and instrument constants. Samples (0.292 mg ml^{-1} 71F6pRNA or 0.370 mg ml^{-1} 71pRNA) were injected at a flow rate of 1 ml min^{-1} in 50 mM Tris–HCl (pH 7.0), 300 mM NaCl. 10 mM $MgCl_2$ plus 0.1 mM EDTA was included in samples where $MgCl_2$ was present. 10 mM EDTA was included in samples where $MgCl_2$ was not present. Precision Acquire 32 and Discovery 32 software (Precision Detectors) was used to record light scattering and UV absorbance chromatograms, to calibrate the experimental set-up and to analyse all data.

AUC

Equilibrium sedimentation experiments were carried out at 14°C using an Optima XL-I Analytical Ultracentrifuge (Beckman). Cells with six-sector centrepieces and quartz windows were placed in a balanced An-60 Ti Analytical Rotor, 4-Place or An-50 Ti Analytical Rotor, 8-Place (Beckman). Samples were initially spun at 3000 r.p.m. and the absorbance recorded to verify sample loading concentration, then at a series of increasing rotor speeds, allowing equilibrium to be reached at each speed. Absorbance profiles were recorded at a wavelength that allowed the concentration of RNA to be monitored without saturating the instrument signal (A < 2.0). Absorbance scans were obtained at regular intervals and equilibrium judged to have been reached when scans did not alter with time. An overspeed run at 45 000 r.p.m. was carried out to deplete the meniscus of all sedimenting species and determine baseline offset values.

Samples of 71pRNA and 120pRNA were prepared in dialysis equilibrium in a range of buffers firstly by dialysis using 0.025 μm pore size membranes (Millipore) followed by concentration on a NAP-5 column (Amersham Biosciences), eluting with the desired buffer. 71pRNA was prepared in a range of buffers: 50 mM Tris–HCl (pH 7.0), (300-3×) mM NaCl, x mM $MgCl_2$ (where $x = 0$, 1, 5 and 10), 0.1 mM EDTA. For each $MgCl_2$ concentration, absorbance profiles were recorded for three samples with concentrations between 0.2 and 1.5 μM in equilibrium sedimentation experiments at 14°C with rotor speeds of 5000, 7000, 10 000 and 13 000 r.p.m. The same experiment was carried out with three samples of 120pRNA at concentrations between 0.1 and 1.0 μM in 50 mM Tris–HCl (pH 7.0), 300 mM NaCl, 10 mM $MgCl_2$ plus 0.1 mM EDTA.

Data at each rotor speed were fitted globally using Optima XL-A/XL-I data analysis software (Beckman) to a single molecular species model:

$$c(r) = c_0 \exp\left[\frac{\omega^2}{2RT} M(1 - \bar{\nu}\rho_o)(r^2 - r_o^2)\right] + \delta \quad \mathbf{1}$$

where c is RNA concentration, r is radius, r_0 is a reference radius, c_0 is the concentration at the reference radius, ω is the angular velocity of the centrifuge, R is the universal gas constant, T is the temperature, M is the MW of the RNA, ρ_o is the solvent density as calculated using the Sednterp software (21) and δ is the baseline offset. A more detailed description for determining $\bar{\nu}$, the partial specific volume, has been published elsewhere (22) and a value of $\bar{\nu} = 0.455$ ml g^{-1} was used in this study. The parameters varied in the fit were c_0 and M.

Data were also fitted to a reversible self-association model including monomer, dimer and trimer species:

$$c(r) = c_{01} e^{\sigma_1 \xi} + c_{01}^2 K_{A1,2} e^{2\sigma_1 \xi} + c_{01}^3 K_{A1,3} e^{3\sigma_1 \xi} + \delta \quad \mathbf{2}$$

where the subscript 1 refers to monomer, $K_{A1,n}$ is the association constant for monomer to the nth oligomeric species, and:

$$\sigma_1 = \frac{M_1(1 - \bar{\nu}\rho_o)\omega^2}{RT} \quad \mathbf{3}$$

and

$$\xi = \frac{r^2 - r_0^2}{2} \quad \mathbf{4}$$

The parameters varied in the fit were the monomeric RNA concentration c_{01} at radius r_0, and the association constants $K_{A1,2}$ and $K_{A1,3}$ for monomer to dimer and monomer to trimer, respectively.

$K_{D2,3}$ values were calculated from $K_{D1,2}$ and $K_{D1,3}$ according to the equation below.

$$K_{D2,3} = \frac{K_{D1,3}}{K_{D1,2}} \quad \mathbf{5}$$

The Gibbs free energy (ΔG^o) for the formation of pRNA multimers was calculated according to:

$$\Delta G^\circ - RT \ln K_A \quad \mathbf{6}$$

where R is the gas constant (1.987 cal K^{-1} mol^{-1}), T is the experimental temperature (287 K for AUC experiments) and K_A is the equilibrium constant for the association event.

SMPB

All buffers and protein samples were confirmed to be free of contaminating fluorescence before use in SMPB experiments. Samples (100 μl) of AF-N-71pRNA and AF-N-CEpRNA in buffer [50 mM Tris, 150 mM NaCl, 10 mM $MgCl_2$ (pH 7.2)] at a concentration of 1 nM (to prevent overlap of fluorescent complexes in the field of view) were immobilized onto a clean glass slide by adsorption for 10 min at room temperature. In the case of experiments with gp10 connector, protein was added to the solution before adsorption to afford a 6:1 pRNA:connector ratio. The slide was washed with an aliquot of buffer, and then overlaid with a 50% solution of PEG400 in buffer. The entirely custom built total internal reflection fluorescence microscope used for these studies is similar to other prismless 'through-the-objective' designs described in the literature (23,24). Briefly, a 488 nm laser beam (Sapphire, Coherent, UK) with a power of ~4 mW is spatially filtered, circularly polarised and then focused to the periphery of the back focal plane of a high numerical aperture oil immersion microscope objective (NA = 1.45, alpha-Plan Fluar, Carl Zeiss, Germany). The emerging light is then incident at or above the critical angle onto the coverglass sample substrate, generating an evanescent field into the aqueous buffer. Fluorescence may then be efficiently excited in molecules near (<150 nm) the surface and the emitted light collected by the same microscope objective. The light is

spectrally filtered to remove Rayleigh and Raman scattered excitation light using a bandpass filter (HQ525/50m, Chroma Tech. Corp., USA). An image is formed onto an electron multiplying CCD camera (iXon, Andor Technology, Northern Ireland) using a single tube lens (acromatic doublet, f = 150 mm). Data were collected simultaneously for up to 30 single complexes adsorbed onto the glass substrate and the surface observed for several minutes with an exposure time of 100 ms per frame. Regions of fluorescence were manually identified in the resulting images and the intensity versus time trajectories analysed, all using custom control and analysis software written in the Igor Pro (Wavemetrics, USA) software package. Sample sizes were 215 for AF-N-pRNA, 169 for AF-N-pRNA + gp10 and 91 for CEpRNA.

Affinity binding assays

C-His gp10 connector [in 10 mM NaH_2PO_4, 0.3 M NaCl, 1 mM imidazole (pH 8.0)] was immobilized on Ni-NTA Magnetic Agarose Beads (Qiagen) by incubation at 4°C for 2 h with gentle agitation. The degree of protein immobilization was quantified by comparing the absorbance of solutions at $\lambda = 280$ nm before and after incubation with magnetic beads. Affinity binding assays (total volume 50 µl) were assembled with 1 nM ^{32}P-labelled RNA (71pRNA, 71F6pRNA or 120pRNA) and bead-bound C-His gp10 (at least 6 concentrations in the range 1–1000 nM) in 10 mM HEPES, 150 mM NaCl (pH 7.4) ± 10 mM $MgCl_2$ and incubated at 20°C for 30 min. As a control for non-specific binding, pRNA interaction with bead-bound histidine-tagged human recombinant superoxide dismutase (His-SOD, Sigma) was used. A magnet was applied to the suspension, the supernatant removed and the resultant bead pellet resuspended in high salt wash buffer [10 mM HEPES, 1 M NaCl (pH 7.4)]. RNA in the high salt wash buffer was ethanol precipitated, resuspended in gel loading buffer and loaded onto a denaturing polyacrylamide gel. Following gel imaging by film exposure and development, bands were quantified using GeneSnap analysis software (Syngene) and the percentage of total RNA bound to beads was calculated relative to a standard. Apparent K_D values were determined by calculating the concentration of bead-bound protein required to bind 50% of the available RNA.

Statistical analysis

Significance (P-values) was analysed by two sample independent t-test using OriginPro 7 (OriginLab Corporation). $P = 0$ for values less than 1×10^{-5}.

RESULTS

pRNA multimerization in solution

Previous studies with wild-type and mutant pRNAs have provided evidence that the pRNA:pRNA interaction is intermolecular and that divalent metal ions are essential for this process. In order to be able to determine the affinity of multimerization, it is essential to first determine the stochiometry of pRNA multimers in solution. To investigate this, we employed light scattering techniques to probe pRNA size and MW in solution (using pRNA variants described in Figure 1B) in the absence of other ϕ29 components. DLS experiments were performed to determine the hydrodynamic radius, R_H, of 71F6pRNA and 71pRNA. An increase in R_H would indicate the presence of higher order pRNA species formed by intermolecular base pairing-directed multimerization. In order to investigate the effect of magnesium ions (Mg^{2+}) on R_H, intensity correlation functions were recorded and size distributions obtained before and after the addition of $MgCl_2$. An additional experiment involved the addition of EDTA to the previously $MgCl_2$-treated samples, providing a control to ensure the specific role of Mg^{2+} in any R_H change.

The R_H distribution of pRNA samples at each stage of Mg^{2+} and EDTA treatment are displayed in Figure 2. The mode average R_H value of 71F6pRNA alone (Figure 2A, red) was 4.3 nm. Addition of 10 mM $MgCl_2$ (green) followed by 10 mM EDTA (blue) resulted in mode R_H values of 4.6 nm and 4.3 nm, respectively, representing a 7% change in distribution mode upon the addition of Mg^{2+}. These data suggest that there was no significant change in R_H under these conditions ($P = 0.67$, two sample independent t-test), consistent with the inability of 71F6pRNA to self-associate via intermolecular base pairing. As well as playing a role in facilitating base pairing, previous studies have suggested that Mg^{2+} may promote a conformational change in pRNA (22,25,26). Although the small ΔR_H on addition of Mg^{2+} may be the result of such a conformational change in the RNA, further analysis would be necessary to confirm this result. In contrast, the mode R_H of 71pRNA (Figure 2B) shifted from 4.2 nm to 5.7 nm ($P = 0$) on the addition of 10 mM $MgCl_2$, representing a 36% increase in 71pRNA size. The specific role of Mg^{2+} in this multimerization was demonstrated by the reduction in R_H on the addition of 10 mM EDTA, when the R_H returns to its original level (5.7 → 4.2 nm, $P = 0$). It is likely that this change in R_H is due to multimerization resulting from Mg^{2+}-dependent intermolecular base pairing. However, it was not possible to ascertain whether pRNA conformational changes were also occurring.

To obtain more information on the pRNA multimerization observed by DLS, SEC-LS was used to quantify the change in formula weight of pRNA species in the presence of Mg^{2+} for both 71pRNA and 71F6pRNA. The separation of RNA species and subsequent determination of their solution formula weights was achieved by injecting each pRNA, in the presence of Mg^{2+}, onto a size exclusion column coupled to light scattering and UV absorbance detectors. The formula weights of the separated species were determined independently by the combination of data from each of these detectors. In this way, formula weight is not dependent on particle shape. The results of SEC-LS assessment of 71F6pRNA and 71pRNA multimerization in the presence of 10 mM $MgCl_2$ are shown (Figure 2C and D). Chromatograms include UV absorbance at 280 nm (blue, UV), light scattering (green, LS) and calculated formula weight (black) at elution times following sample loading and have been normalized so that the main peak maxima of the UV and LS traces coincide.

SEC-LS analysis of the solution state of 71F6pRNA (Figure 2C) reveals the presence of a single species with an elution time of ~8.5 min. As base pair mutations in 71F6pRNA prevent multimerization to form higher order

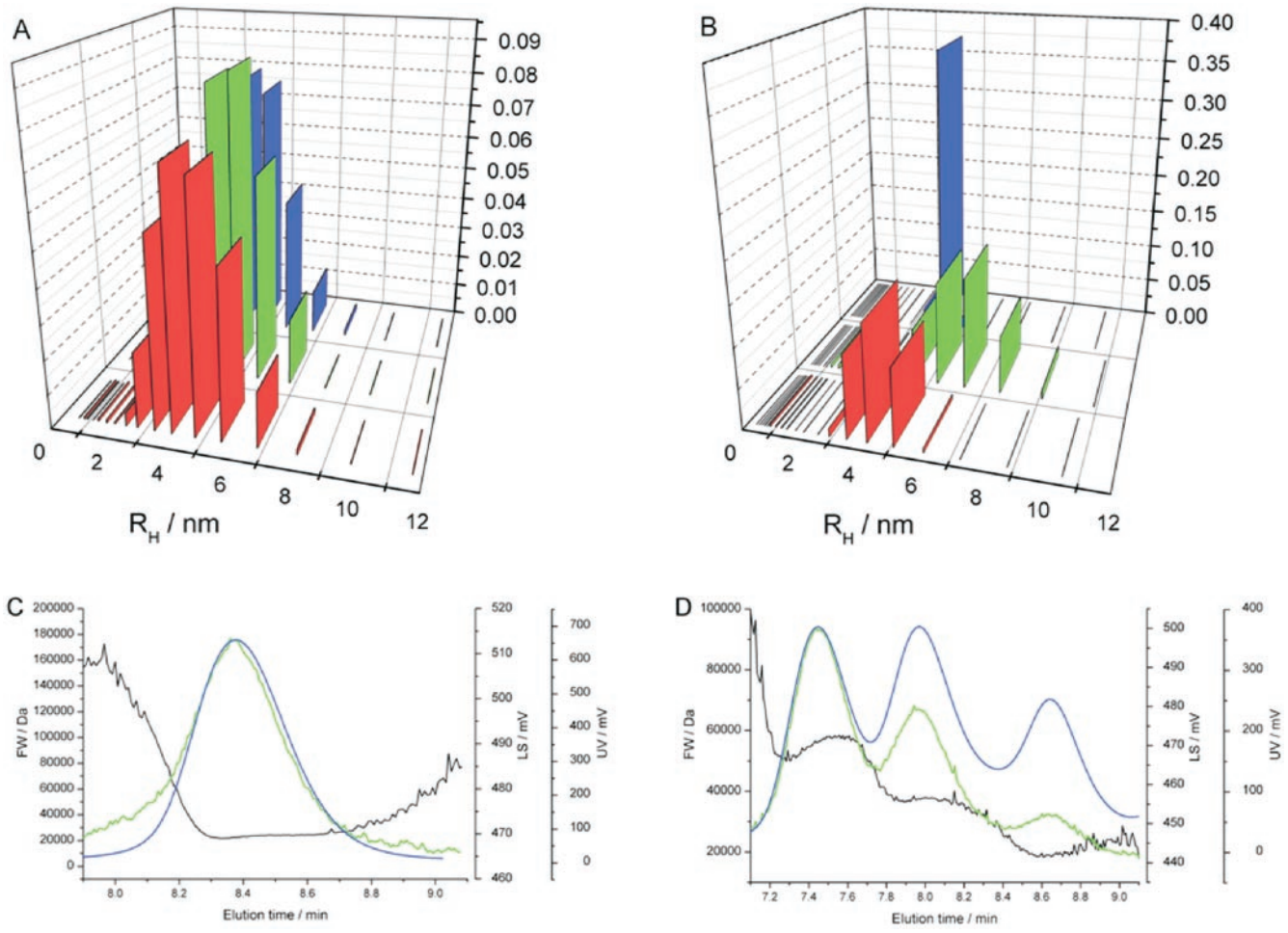

Figure 2. DLS analysis of the solution state multimerization of 71F6pRNA (**A**) and 71pRNA (**B**). The hydrodynamic radius (R_H / nm, plotted against component ratio) of 71F6pRNA (A, red), that lacks complementary bases in the CE and D loops, shows little change on the addition of Mg^{2+} (A, green), or on subsequent addition of EDTA (A, blue). 71pRNA (B, red), with complementary bases in the CE and D loops, forms species of increased R_H on addition of Mg^{2+} (B, green). The addition of EDTA (B, blue) to the solution to sequester free Mg^{2+} ions results in a reversal of this change in R_H. This data is consistent with a 71pRNA multimerization event in the presence of Mg^{2+}, which is not possible in the case of 71F6pRNA. The solution state structure of 71F6pRNA (**C**) and 71pRNA (**D**) in the presence of Mg^{2+} was investigated by SEC-LS, affording accurate formula weight data. Light scattering (C, green) and UV detection (C, blue, 280 nm) of the formula weight of 71F6pRNA Mg^{2+}. (C, black) indicates the presence of a single monomeric species (elutes at 8.4 min). Analysis of 71pRNA. Mg^{2+}. (D) data indicates the presence of three species, equivalent to trimeric (elutes at 7.5 min), dimeric (8.0 min) and monomeric (8.6 min) 71pRNA, as formula weight is proportional to the ratio of LS/UV, and the ratio of the formula weights of each of the three peaks is 3:2:1, in order of earliest elution.

structures, this peak therefore represents the elution time for a monomeric 71 nt RNA with secondary structure equivalent to 71pRNA, and so acts as a standard for the analysis of 71pRNA SEC-LS data. In the case of 71pRNA (Figure 2D), three major species were observed. The LS maximum was equal to that of the UV maximum for the first peak (7.5 min, normalized, as described above), two-thirds for the second peak (8.0 min), and one-third for the third peak (8.6 min). Since the formula weight of each species is proportional to the ratio of the LS and UV traces, this indicates that the ratio of formula weights for the three peaks is 3:2:1. In addition, the third 71pRNA peak eluted at 8.6 min, close to the elution time of monomeric 71F6pRNA (8.4 min). If this 71pRNA peak represents monomeric RNA, the other 71pRNA peaks are dimer (8.0 min) and trimer (7.5 min). Using the calculated monomeric MW and SEC-LS traces of 71F6pRNA to calibrate the instrument, it was possible to calculate the formula weights of the 71pRNA species. The calculated formula weight distribution for the region shown (Figure 2D, black) indicated three main species of formula weights ≈ 55, 37 and 19 kDa, in order of earliest elution. These values coincide, within experimental error, with the calculated formula weights of the 71pRNA trimer, dimer and monomer, indicating that these species are the major solution state components of pRNA in the absence of gp10. Slightly low values for these experimental formula weight values may be due to the low signal to noise ratio in the LS output, and the dependence of formula weight on baseline determination.

pRNA:pRNA affinity in solution

Equilibrium sedimentation experiments provide thermodynamic information about macromolecules in solution,

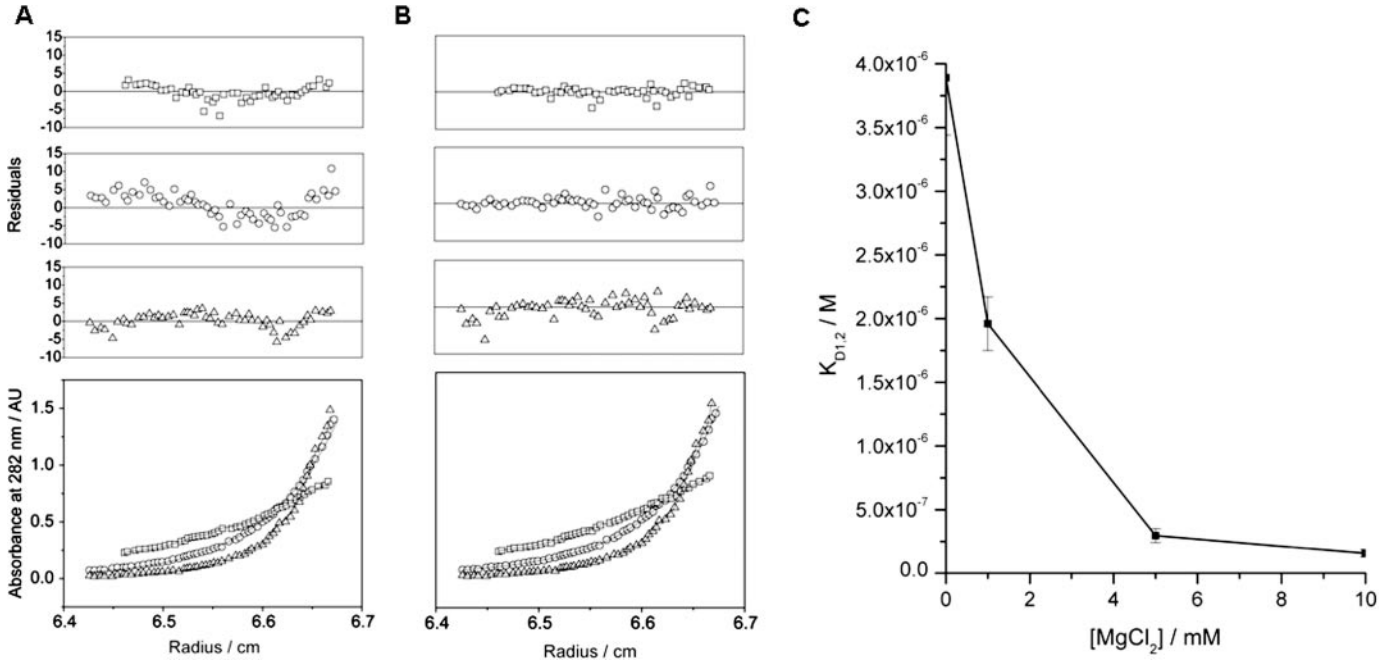

Figure 3. Analysis of multimerization of 71pRNA in the presence of 10 mM Mg^{2+} by equilibrium sedimentation AUC at rotor speeds of 7000 (squares), 10 000 (circles) and 13 000 r.p.m. (triangles). When the data were fitted to a monomeric species model (**A**) the residual plots indicate a significant systematic deviation from zero. In the case of a reversible self-association monomer–dimer–trimer model (**B**), the residuals of the fitted data show no systematic deviation. This model provides dissociation constants for the monomer–dimer interaction of $K_{D1,2} = 0.16$ μM and the dimer–trimer interaction of $K_{D2,3} = 0.42$ μM. The Mg^{2+} concentration dependence of the pRNA multimerization process was probed in the analytical centrifuge by determining K_D values for the multimerization process at a range of Mg^{2+}concentrations. Sub-micromolar affinities are observed for the monomer–dimer interaction at Mg^{2+} concentrations above 5 mM, with a 24-fold reduction in affinity observed in the absence of Mg^{2+} (**C**). K_D confidence limits are indicated as error bars.

including the solution formula weight of the macromolecule and, for associating systems, stoichiometry data and association constants. In order to relate the buoyant formula weights measured in these experiments to the stoichiometries and association constants of multimeric pRNA, it was necessary to obtain an accurate value for the partial specific volume ($\bar{v}$) of pRNA. $\bar{v}$ values for nucleic acids are highly dependent on buffer conditions and vary across a much wider range than those for proteins (27). A detailed description of the measurement of $\bar{v}$ (as 0.455 ml g^{-1}) has been published elsewhere, together with preliminary data on pRNA–pRNA multimerization (22).

In order to further investigate the solution state multimerization of pRNA, a series of sedimentation equilibrium experiments was designed, employing a range of buffers with varying concentrations of Mg^{2+} with each adjusted to ensure a standard overall ionic strength. Data were collected for 71pRNA at a range of concentrations and rotor speeds (7000, 10 000, 13 000 r.p.m. as shown in Figure 3) in buffers with differing concentrations of Mg^{2+}. It is clear from the residual plots that the data for 71pRNA fits poorly to a single species model (Equation 1) over these rotor speeds (Figure 3A), with systematic deviation from zero observed. As the SEC-LS results discussed previously indicated the presence of monomeric, dimeric and trimeric 71pRNA species in the presence of Mg^{2+}, the AUC data for 71pRNA were fitted globally to a reversible self-association model incorporating monomer–dimer–trimer species (Equation 2; Figure 3B). The distribution of residuals under this model is random and less diverse than that of the single species model, indicating a good fit to the data. The parameters varied under the model conditions were concentration and radius, and the association constants $K_{A1,2}$ and $K_{A1,3}$ for monomer to dimer and monomer to trimer, respectively. The dissociation constants $K_{D1,2}$, $K_{D1,3}$ and $K_{D2,3}$ (Table 1) have been calculated from the values of the association constants $K_{A1,2}$ and $K_{A1,3}$ and these values represent the first comprehensive measurements of the affinity of the pRNA multimerization event in solution. $K_{D1,2}$ and $K_{D2,3}$ (for monomer to dimer and dimer to trimer, respectively) for 71pRNA

Table 1. Equilibrium dissociation constants of pRNA multimerization from AUC experiments

[$MgCl_2$] / mM	$K_{D1,2}$ / M D ↔ M	$K_{D2,3}$* / M T ↔ D
71pRNA		
0	3.9×10^{-6} $(3.5, 4.4) \times 10^{-6}$	1.7×10^{-6} $(1.6, 1.8) \times 10^{-6}$
1	2.0×10^{-6} $(1.8, 2.2) \times 10^{-6}$	2.3×10^{-6} $(2.2, 2.4) \times 10^{-6}$
5	3.0×10^{-7} $(2.5, 3.6) \times 10^{-7}$	6.3×10^{-7} $(5.7, 6.7) \times 10^{-7}$
10	1.6×10^{-7} $(1.3, 1.9) \times 10^{-7}$	4.2×10^{-7} $(4.1, 4.3) \times 10^{-7}$
120pRNA		
10	2.6×10^{-7} $(2.1, 3.2) \times 10^{-7}$	3.3×10^{-7} $(2.8, 3.2) \times 10^{-7}$

M = monomer; **D** = dimer; **T** = trimer.
1,2 = monomer–dimer; **2,3** = dimer–trimer.
95% confidence limits derived from experimental values are displayed in brackets.
*derived from $K_{A1,2}$ and $K_{A1,3}$ values.

are in the μM range for all concentrations of Mg^{2+} and it is clear that $K_{D1,2}$ decreases with increasing Mg^{2+} concentration (Figure 3C). In particular, a 24-fold increase in affinity was observed in the presence of 10 mM Mg^{2+} compared to 0 mM Mg^{2+}. This illustrates the Mg^{2+}-dependence of the pRNA monomer to dimer multimerization process and is in agreement with size distribution and formula weight information from light scattering experiments described previously. Interestingly, the value for $K_{D2,3}$, representing the dimer–trimer interaction, shows less Mg^{2+} dependence: a 4-fold increase in affinity was observed in the presence of 10 mM Mg^{2+} compared to in the absence of Mg^{2+}, although the error in this calculation is larger as it combines the uncertainties in the measurements of both $K_{A1,2}$ and $K_{A1,3}$.

Analogous analyses were performed to determine association constants for the solution state multimerization of 120pRNA in the presence of 10 mM Mg^{2+}. The quality of the fit for 120pRNA data was similar to that of 71pRNA using a reversible self-association model (22) and the determined association constants are comparable to those of 71pRNA (Table 1). For example $K_{D1,2}$ for the monomer–dimer interaction is 0.16 μM for 71pRNA and 0.26 μM for 120pRNA. The A helix which is present in 120pRNA, but greatly shortened in 71pRNA (Figure 1B), appears to have little or no effect on the affinity constants describing multimerization.

pRNA multimerization and interaction with connector

Although pRNA alone in solution does not multimerize beyond trimer, it is likely that more than three pRNAs bind to each connector during DNA packaging (13,28). In order to probe a possible role of gp10 connector in the stabilization of pRNA multimers with order higher than three, SMPB experiments were performed. These experiments involved the analysis of the SMPB of individual complexes containing fluorophore-labelled RNA molecules: the number of photobleaching events observed for a particular fluorescent complex correlates to the number of fluorophore-labelled RNA molecules within a complex (29–31). The multimerization of pRNA in the presence of Mg^{2+} was probed with and without C-His gp10 connector (Figure 4A).

The CE region of pRNA (Figure 1B) labelled with AlexaFluor 488, was selected as a non-multimerizing control for these experiments. Analysis of the photobleaching distribution of AF-N-CEpRNA in the presence of Mg^{2+} (Figure 4B, grey) indicates that ~90% of the fluorescent features contain a single photobleaching event, and is representative of a system in which monomeric species dominate. An equivalent analysis of data for the 71pRNA probe, AF-N-71pRNA (Figure 4B, white), indicates the presence of a higher proportion of multiple step bleaching events. In particular the presence of fluorescent regions with two and three photobleaching events indicates that ~50% of the complexes within the 71pRNA sample are present as dimers and trimers. Very few complexes with order higher than trimer were observed in the case of AF-N-71pRNA, as expected from the SEC-LS experiments. The number of bleaching steps in fluorophore-labelled pRNA molecules provides evidence for pRNA multimerization equivalent to that described previously, and it is therefore unlikely that the fluorophore is affecting pRNA multimerization. To study interactions between pRNA and gp10 connector, AF-N-71pRNA plus 10 mM Mg^{2+} was incubated with connector prior to analysis (Figure 4B, black). In addition to fluorescent features with one, two and three photobleaching events, four or more photobleaching events were also observed in 8% of the complexes present. These events are indicative of the presence of complexes containing four or more fluorophore-labelled pRNA molecules, and their presence in only 2% of complexes in experiments in the absence of connector protein indicates the direct involvement of the connector in the assembly of higher order pRNA multimers. While these observed complexes do not represent a high proportion of the total number of complexes, they are considerable in view of the very low pRNA concentration under which the experiments were completed.

pRNA:connector affinity

Bead-based affinity binding assays have been used to obtain apparent K_D (K_{Dapp}) values for the interaction between variant pRNA species and connector in the presence and absence of Mg^{2+}. An assay adapted from Bae *et al*. (32) has been used in which one component of the interaction (C-His gp10 connector) was immobilized onto magnetic beads via Ni^{2+} interaction. This allows simple addition and removal of the protein component of the interaction by the use of a magnet. The RNA species used in this assay were labelled with ^{32}P during transcription to allow quantitation following completion of the binding assay. All affinity binding assays were completed in the presence and absence of Mg^{2+} to determine the role of magnesium ions in the pRNA:connector interaction. Binding curves representing the six different experimental conditions (Figure 5) were used to calculate the apparent K_D of each interaction. Assays were repeated in triplicate for each RNA and magnesium ion condition to allow the calculation of averaged values with error parameters (Table 2). In the presence of Mg^{2+}, the affinity of connector for 71pRNA and 120pRNA exhibit $K_{Dapp} = 15 \pm 1$ nM and $K_{Dapp} = 11 \pm 1$ nM, respectively. In contrast in the absence of Mg^{2+}, $K_{Dapp} = 380 \pm 14$ nm and $K_{Dapp} = 350 \pm 10$ nM for 71pRNA and 120pRNA, respectively, a greater than 25-fold decrease in affinity for both species. In the case of 71F6pRNA, which lacks the ability to form pRNA:pRNA interactions, $K_{Dapp} = 55 \pm 4$ nM in the presence of Mg^{2+} and $K_{Dapp} = 940 \pm 20$ nM in the absence of Mg^{2+}, representing an ~17-fold decrease in affinity. This minor 5-fold reduction in affinity between 120pRNA and 71F6pRNA implies that pRNA multimerization is not essential for binding to connector despite it being essential for DNA packaging by ϕ29. In a control assay, binding of pRNA to histidine-tagged human recombinant superoxide dismutase was not observed.

DISCUSSION

We have investigated the solution state of ϕ29 pRNA and the affinity of both pRNA self-association and formation of the gp10 connector:pRNA complex.

The solution state multimerization of 71pRNA has been investigated by DLS and SEC-LS, indicating that this RNA

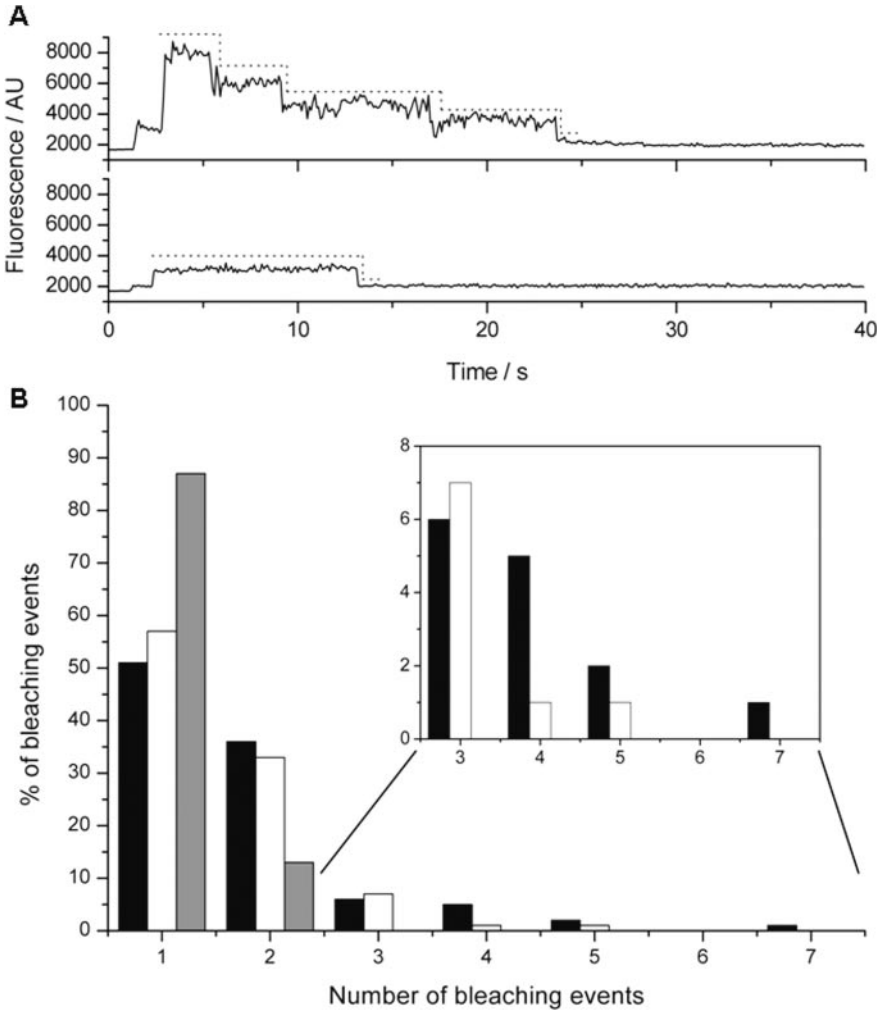

Figure 4. Example traces showing fluorophore photobleaching for AF-N-71pRNA +10 mM Mg^{2+} + C-His gp10 connector (**A**), upper and AF-N-CEpRNA + 10 mM Mg^{2+} (**A**), lower. The dashed line provides an indication of the steps identified in this particular trace and used in data analysis. Data from SMPB experiments were analysed by determining the number of photobleaching events observed in different experimental assemblies (**B**). In the case of AF-N-CEpRNA + 10 mM Mg^{2+} (grey), which has no inherent ability to multimerize, ~90% of the photobleaching events represent monomeric species. When the number of photobleaching events for AF-N-71pRNA + 10 mM Mg^{2+} is analysed (white), there is an increase in the proportion of dimeric species observed and a significant number of pRNA trimers are also present. A stabilization of higher order pRNA species is observed as an increase in the occurrence of four or more photobleaching events (inset shows enlarged view of higher order region of histogram) when AF-N-71pRNA + 10 mM Mg^{2+} is incubated with gp10 connector (black).

exists in monomeric, dimeric and trimeric forms in Mg^{2+}-dependent equilibrium. The removal of complementary bases in the CE loop to form 71F6pRNA resulted in the presence of only monomeric species in solution, in both the presence and absence of Mg^{2+}. In these light scattering experiments, there was no evidence for any higher order assembly of 71pRNA than trimer, even when pRNA was present in higher concentrations. This is in contrast to published gel electrophoresis data (12,13) that demonstrate the presence of hexamers, although it has since been reported that the production of such RNA ladders requires unusual conditions (28) and thus these data may not reflect the solution state of the molecule. The involvement of pRNA dimers in DNA packaging has been extensively reported (12,28). In addition, in cases where mutants have been designed with CE and D loops that base pair to form closed trimers, these species were still competent to bind to proheads (33). Although we do not know whether the trimers seen in our experiments are open or closed structures, it is possible that these molecules may be an important component in the assembly of the ϕ29 packaging motor.

A comprehensive analysis of the solution state pRNA:pRNA multimerization process in the absence of other components of the ϕ29 packaging motor by AUC has resulted in the first measurements of the affinity of pRNA self-association in solution at a range of magnesium ion concentrations. The K_D values were in the μM range, with a 24-fold increase in affinity in the monomer–dimer 71pRNA interaction observed following the addition of 10 mM Mg^{2+}, while the dimer–trimer association process showed a less pronounced Mg^{2+}-dependence. The equilibrium constants for the multimerization events (Table 1) have been used to calculate (Equation 6) the Gibbs free energy change for the formation of dimer species from

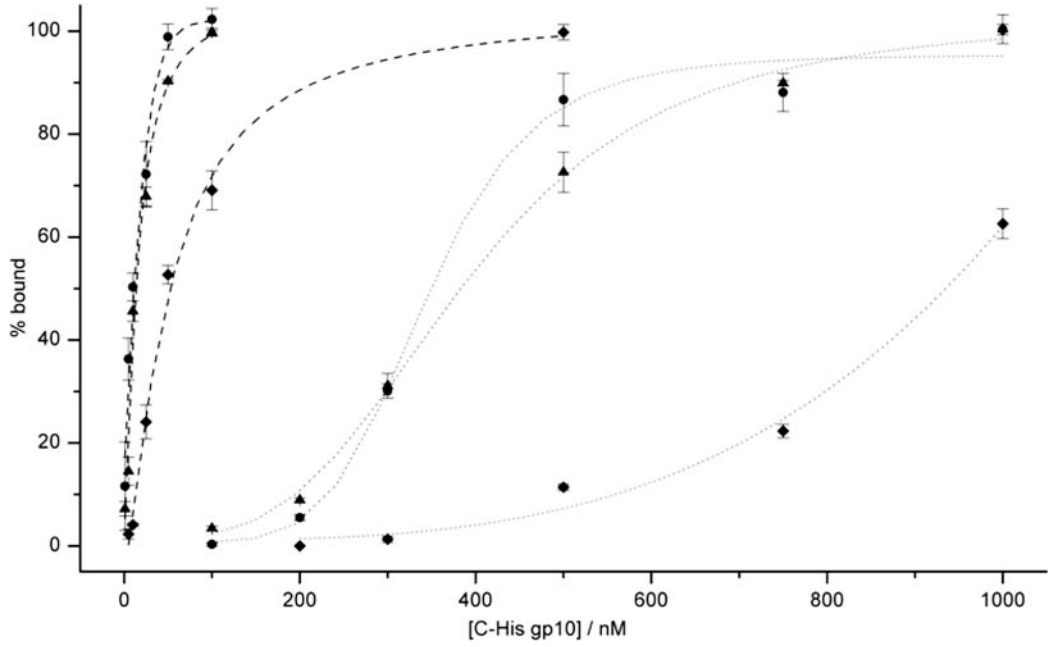

Figure 5. Data from affinity binding assays to determine the affinity between C-His gp10 connector and pRNA in the presence (dashed lines) and absence (dotted lines) of Mg^{2+} (71pRNA = triangle, 120pRNA = circle and 71F6pRNA = diamond). 71pRNA + Mg^{2+} and 120pRNA + Mg^{2+} have K_{Dapp} = 15 nM and 11 nM, respectively, whereas 71F6pRNA + Mg^{2+} has K_{Dapp} = 55 nM. In contrast in the absence of Mg^{2+}, the K_{Dapp} values for 71pRNA and 120pRNA are greater than 350 nM and for 71F6pRNA, K_{Dapp} = 940 nM.

Table 2. Equilibrium dissociation constants of the pRNA:connector interaction from affinity binding assays

	K_{Dapp} / M $+Mg^{2+}$	$-Mg^{2+}$
71pRNA	$1.5 \pm 0.1 \times 10^{-8}$	$3.8 \pm 0.1 \times 10^{-7}$
120pRNA	$1.1 \pm 0.1 \times 10^{-8}$	$3.5 \pm 0.1 \times 10^{-7}$
71F6pRNA	$5.5 \pm 0.4 \times 10^{-8}$	$9.4 \pm 0.2 \times 10^{-7}$

monomeric 71pRNA. $\Delta G^{\circ}_{1,2} = -7.1$ kcal mol^{-1} for 71pRNA in the absence of magnesium ions. Of particular interest is the effect of the presence of Mg^{2+} on $\Delta G^{\circ}_{1,2}$ for 71pRNA: $\Delta\Delta G^{\circ}_{1,2} = -1.8$ kcal mol^{-1} on the addition of 10 mM Mg^{2+} to the system. AUC analysis of 120pRNA in the presence of 10 mM Mg^{2+} provided evidence that the A helix of 120pRNA (truncated in 71pRNA) has little influence on the affinity of pRNA multimerization, with a similar μM range monomer–dimer affinity observed to that for 71pRNA. These values represent a minimal difference in Gibbs free energy between 71pRNA and 120pRNA ($\Delta\Delta G^{\circ}_{1,2} = 0.3$ kcal mol^{-1}) for the formation of the dimeric species, and suggest that 71pRNA provides an excellent model for the study of 120pRNA multimerization. The lack of contribution of the A helix to the affinity of pRNA:pRNA interaction is in agreement with recent studies designed to measure the affinity of the pRNA multimerization process (34). By quantifying the multimerization event using native gel assays, values for the monomer–dimer event of K_D = 21.7 nM and $\Delta G^{\circ} = -10.2$ kcal mol^{-1} were obtained. These values indicate a higher affinity for multimerization than those reported here, in which we have particular confidence due to the true solution state nature of the AUC technique. Moreover, the experiments described here investigate wild-type loop base pairing, rather than the mutants used previously (34) which enforce the formation of specific multimers with an increased number of G-C base pairs in the loop:loop interactions. This sequence change results in a possible addition of two hydrogen bonds contributing to the intermolecular dimer contacts, each of which may contribute 0.5–1.8 kcal mol^{-1} to the ΔG° for the interaction (35,36).

A previous report attempted to use AUC to determine the stoichiometry of pRNA multimers (12). Data for 120pRNA was fitted using an assumed value of $\bar{v}$ to a model including three different species: monomer, dimer and hexamer. We believe that our data represent a more comprehensive and accurate analysis; we investigated the effects of buffer composition and an accurately determined value of $\bar{v}$ was used for the analysis (22), thus allowing the measured buoyant formula weight to be correlated to actual formula weights of multimeric species.

SMPB experiments have been used to confirm the solution state mutimerization of pRNA and demonstrate the role of connector protein in the further stabilization of higher order species. AF-N-71pRNA forms monomeric, dimeric and trimeric species in the presence of Mg^{2+} as indicated by the predominance of one, two and three photobleaching events in the datasets. In contrast AF-N-CEpRNA, consisting of only one of the two loops necessary for intermolecular multimerization, exhibited predominantly monomeric character. On analysis of AF-N-71pRNA in the presence of gp10 connector, photobleaching traces with four or more steps were observed. These results indicate that gp10 connector may act as a scaffold for the assembly of higher order pRNA multimers.

The interaction of pRNA species with gp10 connector has been probed in more detail by affinity binding assays. The

affinity of all pRNA species was increased when Mg^{2+} was present. The apparent K_D (K_{Dapp}) of the 120pRNA: connector interaction was shown to be 0.35 μM, increasing in the presence of Mg^{2+} to 11 nM. A similar trend was measured for 71pRNA (0.38 μM to 15 nM). In the case of a non-multimerizing pRNA, 71F6pRNA, a K_{Dapp} of 0.94 μM was observed, increasing to 55 nM in the presence of Mg^{2+}, indicating that an ability to multimerize is not essential for the binding of pRNA to connector. This conclusion is supported by work with circularly permuted pRNAs, where disruption of the loops involved in intermolecular base pairing still resulted in procapsid interaction (37). Scatchard plots of the data revealed no evidence of co-operative binding under these conditions. However, in order to perform equilibrium binding assays of this type, it is essential to keep the RNA concentration as low as possible (10-fold lower than the K_{Dapp}) to obtain meaningful data, and as a consequence it is possible that individual connectors are not fully saturated with RNA. Control experiments in affinity binding assays have shown this pRNA:connector interaction to be specific, as binding of pRNA to His-SOD was not observed.

These are the first measurements of the K_D of the interaction between pRNA and connector, although some data describing binding to prohead has been previously documented. Competition assays employing the 120 nt variant of 71F6pRNA (11) resulted in the loss of 80% of activity. The use of a different multimerization-defective mutant in binding and competition assays resulted in similar reduction and a binding affinity of 80 nM between wild-type pRNA and prohead was reported as a result of Hill plot analysis (28). The data presented here demonstrate clearly that pRNA mutimerization is not essential for connector binding, but suggest a link between conformation and the ability to bind to the connector. pRNAs that are competent to self-associate (71pRNA or 120pRNA) bind with similar affinity and the mutant that cannot self-associate (71F6pRNA) binds with only a 5-fold reduction in affinity. However, the affinity of all of the RNAs is decreased in the absence of Mg^{2+}, consistent with a requirement for a Mg^{2+}-dependent conformational change for optimal binding of pRNA to connector.

These new data provide new insight toward the development of a model of ϕ29 genomic DNA packaging. The high affinity (nM K_D) between pRNA and connector in the presence of magnesium ions indicates that it is unlikely that a pRNA multimer would rotate around the connector during DNA packaging. It also seems unlikely that, after association of a hexameric pRNA ring to the connector, one RNA molecule is lost from the complex [as proposed by Simpson *et al.* (8)] as this would involve loss of both pRNA–pRNA and pRNA–connector interactions. It is, however, possible that the motor is driven by conformational change. The data presented here are supported by previous studies indicating pRNA conformational changes in the presence of Mg^{2+} (13,22,25,26). However, these are the first experiments that demonstrate a Mg^{2+}-dependent effect on the affinity of connector interactions by a multimerization-incompetent pRNA, therefore indicating that this effect cannot be related to pRNA self-association alone. This observation does not exclude the possibility that pRNA is involved in self-association before interaction with the connector, but indicates that this event may contribute less to the overall assembly than previously suggested (12,28). Based on previous studies together with the data reported here, we propose a model for motor function. This involves a conformational change which brings about localized distortion of the connector portal, resulting in DNA packaging. The model would hold with the involvement of any number of pRNA molecules forming a closed ring as part of the motor. A conformational change in one pRNA, possibly coupled to ATPase activity, would alter its contact to the connector, promoting a localized distortion in the connector and hence translocation of genomic DNA into the procapsid. This would also set-up a distortion of the pRNA ring which would help to promote conformational change in the adjacent pRNAs, propagating further packaging motor activity. Further analysis of molecular interactions at different stages of the packaging process are clearly required to develop a full understanding of this DNA packaging machine.

ACKNOWLEDGEMENTS

This work was supported by the BBSRC (UK), the MRC (UK) and the University of Leeds. The authors wish to thank Dr A.E. Ashcroft for mass spectrometry analysis and Prof. P. Guo for the gift of pAR7-8-8.5-10 and useful discussions. Funding to pay the Open Access publication charges for this article was provided by The University of Leeds.

Conflict of interest statement. None declared.

REFERENCES

1. Smith,D.E., Tans,S.J., Smith,S.B., Grimes,S., Anderson,D.L. and Bustamante,C. (2001) The bacteriophage ϕ29 portal motor can package DNA against a large internal force. *Nature*, **413**, 748–752.
2. Chemla,Y.R., Aathavan,K., Michaelis,J., Grimes,S., Jardine,P.J., Anderson,D.L. and Bustamante,C. (2005) Mechanism of force generation of a viral DNA packaging motor. *Cell*, **122**, 683–692.
3. Lee,C.-S. and Guo,P. (1995) *In vitro* assembly of infectious virions of double-stranded DNA phage ϕ29 from cloned gene products and synthetic nucleic acids. *J. Virol.*, **69**, 5018–5023.
4. Hendrix,R.W. (1978) Symmetry mismatch and DNA packaging in large bacteriophages. *Proc. Natl Acad. Sci. USA*, **75**, 4779–4783.
5. Serwer,P. (2003) Models of bacteriophage DNA packaging motors. *J. Struct. Biol.*, **141**, 179–188.
6. Guasch,A., Pous,J., Parraga,A., Valpuesta,J.M., Carrascosa,J.L. and Coll,M. (1998) Crystallographic analysis reveals the 12-fold symmetry of the bacteriophage ϕ29 connector particle. *J. Mol. Biol.*, **281**, 219–225.
7. Valpuesta,J.M., Fernandez,J.J., Carazo,J.M. and Carrascosa,J.L. (1999) The three-dimensional structure of a DNA translocating machine at 10 Å resolution. *Struct. Fold. Des.*, **7**, 289–296.
8. Simpson,A.A., Tao,Y.Z., Leiman,P.G., Badasso,M.O., He,Y.N., Jardine,P.J., Olson,N.H., Morais,M.C., Grimes,S., Anderson,D.L. *et al.* (2000) Structure of the bacteriophage ϕ29 DNA packaging motor. *Nature*, **408**, 745–750.
9. Guasch,A., Pous,J., Ibarra,B., Gomis-Ruth,F.X., Valpuesta,J.M., Sousa,N., Carrascosa,J.L. and Coll,M. (2002) Detailed architecture of a DNA translocating machine: the high-resolution structure of the bacteriophage ϕ29 connector particle. *J. Mol. Biol.*, **315**, 663–676.
10. Guo,P., Erickson,S. and Anderson,D. (1987) A small viral-RNA is required for *in vitro* packaging of bacteriophage ϕ29 DNA. *Science*, **236**, 690–694.
11. Reid,R., Zhang,F., Benson,S. and Anderson,D. (1994) Probing the structure of bacteriophage ϕ29 prohead RNA with specific mutations. *J. Biol. Chem.*, **269**, 18656–18661.

12. Zhang,F., Lemieux,S., Wu,X.L., St Arnaud,D., McMurray,C.T., Major,F. and Anderson,D. (1998) Function of hexameric RNA in packaging of bacteriophage ϕ29 DNA *in vitro*. *Mol. Cell*, **2**, 141–147.
13. Guo,P., Zhang,C., Chen,C., Garver,K. and Trottier,M. (1998) Inter-RNA interaction of phage ϕ29 pRNA to form a hexameric complex for viral DNA transportation. *Mol. Cell*, **2**, 149–155.
14. Ibarra,B., Caston,J.R., Llorca,O., Valle,M., Valpuesta,J.M. and Carrascosa,J.L. (2000) Topology of the components of the DNA packaging machinery in the phage ϕ29 prohead. *J. Mol. Biol.*, **298**, 807–815.
15. Guo,P., Bailey,S., Bodley,J.W. and Anderson,D. (1987) Characterization of the small RNA of the bacteriophage ϕ29 DNA packaging machine. *Nucleic Acids Res.*, **15**, 7081–7090.
16. Limbach,P.A., Crain,P.F. and McCloskey,J.A. (1995) Molecular mass measurements of intact ribonucleic acids via electrospray ionization quadrupole mass spectrometry. *J. Am. Soc. Mass Spectrom.*, **6**, 27–39.
17. Scaringe,S.A., Wincott,F.E. and Caruthers,M.H. (1998) Novel RNA synthesis method using 5′-O-silyl-2′-O-orthoester protecting groups. *J. Am. Chem. Soc.*, **120**, 11820–11821.
18. Tsuprun,V., Anderson,D. and Egelman,E.H. (1994) The bacteriophage ϕ29 head-tail connector shows 13-fold symmetry in both hexagonally packed arrays and as single particles. *Biophys. J.*, **66**, 2139–2150.
19. Guo,P., Erickson,S., Xu,W., Olson,N., Baker,T.S. and Anderson,D. (1991) Regulation of the phage ϕ29 prohead shape and size by the portal vertex. *Virology*, **183**, 366–373.
20. Stonehouse,N.J. and Stockley,P.G. (1993) Effects of amino acid substitution on the thermal stability of MS2 capsids lacking genomic RNA. *FEBS Lett.*, **334**, 355–359.
21. Laue,T., Shah,B., Ridgeway,T. and Pelletier,S. (1992) Computer-aided Interpretation of Sedimentation Data for Proteins in Harding, S.E., Rowe, A.J., Horton, J.C. (ed.),. *Analytical Ultracentrifugation in Biochemistry and Polymer Science*. Royal Society of Chemistry, Cambridge, pp. 90–125.
22. Wood,J.P.A., Capaldi,S.A., Robinson,M.A., Baron,A.J. and Stonehouse,N.J. (2005) RNA multimerisation in the DNA packaging motor of bacteriophage ϕ29. *J. Theor. Med.*, **6**, 127–134.
23. Conibear,P.B. and Bagshaw,C.R. (2000) A comparison of optical geometries for combined flash photolysis and total internal reflection fluorescence microscopy. *J. Microsc.*, **200**, 218–229.
24. Mashanov,G.I., Tacon,D., Knight,A.E., Peckham,M. and Molloy,J.E. (2003) Visualizing single molecules inside living cells using total internal reflection fluorescence microscopy. *Methods*, **29**, 142–152.
25. Chen,C. and Guo,P. (1997) Magnesium-induced conformational change of packaging RNA for procapsid recognition and binding during phage ϕ29 DNA encapsidation. *J. Virol.*, **71**, 495–500.
26. Trottier,M., Mat-Arip,Y., Zhang,C.L., Chen,C.P., Sheng,S.T., Shao,Z.F. and Guo,P.X. (2000) Probing the structure of monomers and dimers of the bacterial virus ϕ29 hexamer RNA complex by chemical modification. *RNA*, **6**, 1257–1266.
27. Eisenberg,H. (1994) Protein and nucleic-acid hydration and cosolvent interactions—establishment of reliable base-line values at high cosolvent concentrations. *Biophys. Chem.*, **53**, 57–68.
28. Chen,C.P., Sheng,S.T., Shao,Z.F. and Guo,P.X. (2000) A dimer as a building block in assembling RNA—a hexamer that gears bacterial virus ϕ29 DNA-translocating machinery. *J. Biol. Chem.*, **275**, 17510–17516.
29. Ying,L. and Xie,X.S. (1998) Fluorescence spectroscopy, exciton dynamics, and photochemistry of single allophycocyanin trimers. *J. Phys. Chem. B*, **102**, 10399–10409.
30. Abe,K., Kaya,S., Hayashi,Y., Imagawa,T., Kikumoto,M., Oiwa,K., Katoh,T., Yazawa,M. and Taniguchi,K. (2003) Correlation between the activities and the oligomeric forms of pig gastric H/K-ATPase. *Biochemistry*, **42**, 15132–15138.
31. Gordon,M.P., Ha,T. and Selvin,P.R. (2004) Single-molecule high resolution imaging with photobleaching. *Proc. Natl Acad. Sci. USA*, **101**, 6462–646.
32. Bae,S.-J., Oum,J.-H., Sharma,S., Park,J. and Lee,S.-W. (2002) *In vitro* selection of specific RNA inhibitors of NFATc. *Biochem. Biophys. Res. Commun.*, **298**, 486–492.
33. Shu,D., Huang,L.P., Hoeprich,S. and Guo,P.X. (2003) Construction of ϕ29 DNA-packaging RNA monomers, dimers, and trimers with variable sizes and shapes as potential parts for nanodevices. *J. Nanosci. Nanotech.*, **3**, 295–302.
34. Fang,Y., Cai,Q. and Qin,P.Z. (2005) The procapsid binding domain of ϕ29 packaging RNA has a modular architecture and requires 2′-hydroxyl groups in packaging RNA interaction. *Biochemistry*, **44**, 9348–9358.
35. Fersht,A.R. (1988) Relationships between apparent binding energies measured in site-directed mutagenesis experiments and energetics of binding and catalysis. *Biochemistry*, **27**, 1577–1580.
36. Murray,J.B., Adams,C.J., Arnold,J.R.P. and Stockley,P.G. (1995) The roles of the conserved pyrimidine bases in hammerhead ribozyme catalysis: evidence for a magnesium ion-binding site. *Biochem. J.*, **311**, 487–494.
37. Zhang,C., Tellinghuisen,T. and Guo,P. (1997) Use of circular permutation to assess six bulges and four loops of DNA-packaging pRNA of bacteriophage ϕ29. *RNA*, **3**, 315–323.
38. Mathews,D.H., Sabina,J., Zuker,M. and Turner,D.H. (1999) Expanded sequence dependence of thermodynamic parameters improves prediction of RNA secondary structure. *J. Mol. Biol.*, **288**, 911–940.
39. Zuker,M. (2003) Mfold web server for nucleic acid folding and hybridization prediction. *Nucleic Acids Res.*, **31**, 3406–3415.